Geophysical Research Letters

RESEARCH LETTER
10.1029/2023GL103553

Photoferrotrophic Bacteria Initiated Plate Tectonics in the Neoarchean

Shengxing Zhang[1,2,3], Yiliang Li[2,3], Wei Leng[1,3], and Michael Gurnis[4]

[1]Laboratory of Seismology and Physics of Earth's Interior, School of Earth and Space Sciences, University of Science and Technology of China, Hefei, China, [2]Department of Earth Sciences, The University of Hong Kong, Hong Kong, China, [3]CAS Center for Excellence in Comparative Planetology, Hefei, China, [4]Seismological Laboratory, California Institute of Technology, Pasadena, CA, USA

Key Points:

- The biologically induced deposition of magnetite-rich banded iron formations (BIFs) at proto-continental margins can initiate plate tectonics
- The peak deposition of BIFs in 2.75–2.4 Ga indicates the onset time of plate tectonics
- Biological activities have an important influence on the tectonic behavior of Earth

Supporting Information:

Supporting Information may be found in the online version of this article.

Correspondence to:

Y. Li and W. Leng,
yiliang@hku.hk;
wleng@ustc.edu.cn

Citation:

Zhang, S., Li, Y., Leng, W., & Gurnis, M. (2023). Photoferrotrophic bacteria initiated plate tectonics in the Neoarchean. *Geophysical Research Letters*, *50*, e2023GL103553. https://doi.org/10.1029/2023GL103553

Received 7 MAR 2023
Accepted 5 MAY 2023

Abstract Plate tectonics distinguishes Earth from the other terrestrial planets but its initiation mechanism and onset time are debated. We propose plate tectonics was initiated by the deposition of magnetite-rich banded iron formations (BIFs) through biogeochemical iron cycling in Neoarchean oceans. In the photic zone of proto-continental margins, photoferrotrophic bacteria efficiently oxidized the dissolved Fe(II) and induced massive precipitation of ferric oxyhydroxide, which would rapidly react with Fe(II)-rich hydrothermal fluids from coeval vigorous volcanism in Neoarchean oceans to produce magnetite-rich BIFs. Mechanical models demonstrate that the localization of high-density BIF deposition near proto-continents induces collapse of the lithosphere and can initiate the earliest subduction. The peak deposition of BIFs in 2.75–2.40 Ga provides a time constraint on the inception of plate tectonics.

Plain Language Summary Plate tectonics provides a basic framework for understanding geological processes on Earth. Although the subduction of cold and heavy oceanic lithosphere can maintain the operation of plate tectonics, its initiation mechanism remains unclear. To reveal the origin mystery of plate tectonics, it is necessary to clarify how and when the first subduction on Earth began. In this study, we propose a hypothetical model that links Earth's biological processes with the origin of plate tectonics. In the photic zone of the Neoarchean continental margins, the anaerobic metabolism of photoferrotrophic bacteria greatly promoted the massive deposition of magnetite-rich banded iron formations (BIFs). Our mechanical calculations show that within an acceptable sedimentary thickness, these heavy BIF deposits can provide enough downward force to rupture the Neoarchean continental margins and initiate the earliest subduction. The peak deposition of BIFs in 2.75–2.4 Ga further implies the onset time of global plate tectonics.

1. Introduction

Plate tectonics provides a powerful description of the kinematics of the solid Earth and plays a fundamental role in supporting the energy, mass, and chemical cycling since its onset. However, when and how plate tectonics began has been a focus of research since its discovery (Cawood et al., 2018; Condie & Kröner, 2008; Korenaga, 2013). A number of mechanisms have been proposed to explain the onset of subduction and in turn, plate tectonics (T. V. Gerya et al., 2015; Hansen, 2007; Rey et al., 2014). Processes that localize both driving forces and lithospheric weakening are likely required. The weakening of lithosphere could occur through a combination of grain damage, grain-size reduction, thermal processes, and mineralogic change through reaction with water (Escartín et al., 2001; Mulyukova & Bercovici, 2017; Poirier, 1980; Thielmann & Kaus, 2012). External processes such as meteorite impacts have been suggested to break up the lithosphere and initiate subduction (Hansen, 2007). Interior geodynamic processes such as mantle plumes (T. V. Gerya et al., 2015) and the spreading of buoyant continents (Rey et al., 2014) have also been proposed as the nucleating processes of the earliest subduction. The mantle-plume model requires impingement of a hot plume head to rupture the lithosphere, while the continent-spreading model emphasizes that a thick and buoyant continent is gravitationally unstable and its lateral collapse may induce subduction. These models primarily examined pure geophysical processes, while overlooking the possible influence of a young biosphere on the solid Earth which is distinctive among all the terrestrial planets. Besides, these models did not provide a decisive time constraint for the origin of plate tectonics.

The influence of thick sediments on subduction initiation within modern continental margin settings has long been proposed (Cloetingh et al., 1982; Erickson, 1993), but the results show that the force associated with

10.1029/2023GL103553

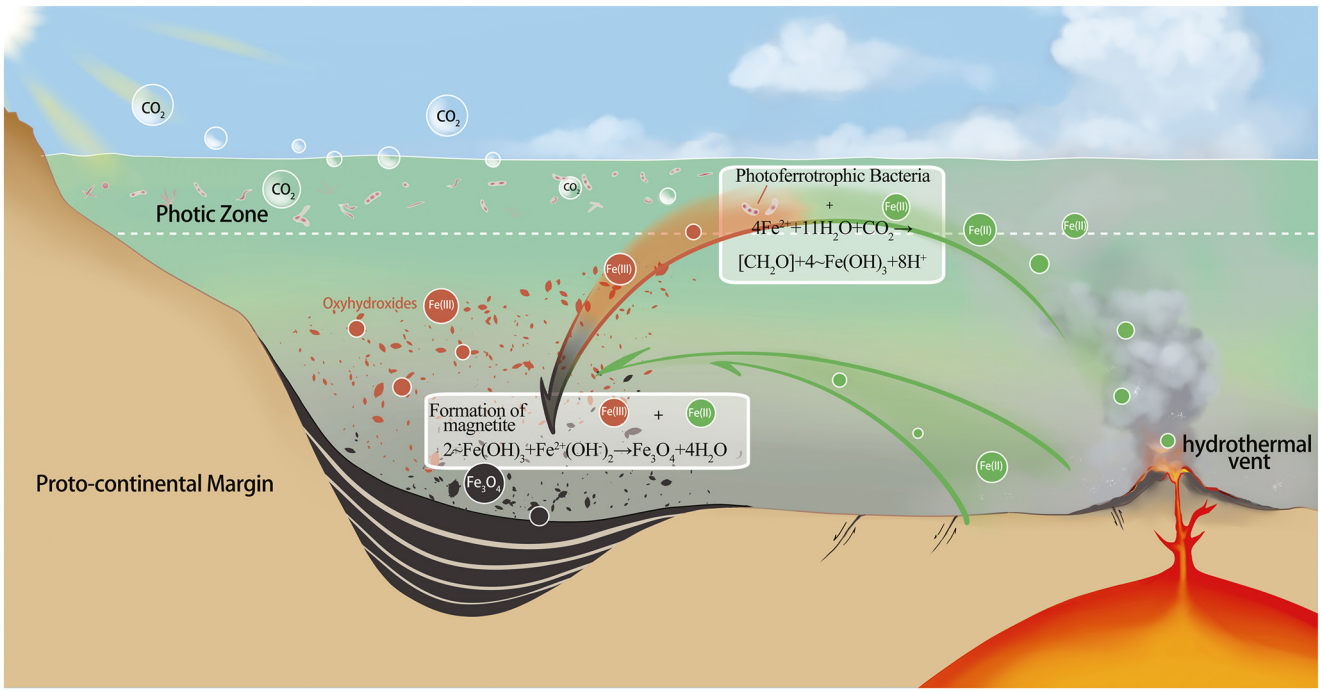

Figure 1. Schematic diagram showing the formation of magnetite-rich BIFs on the Neoarchean continental margins facilitated by the photoferrotrophic bacteria. The Fe(II) is supplied by hydrothermal vents, which may originate from submarine volcanoes caused by the general thermal activity within Earth's interior.

low-density (~2,400 kg/m^3) silicate sediments cannot rupture a mature passive margin (Cloetingh et al., 1982). Here, we argue that the banded iron formation (BIF), an early Precambrian iron-rich sedimentary rock, could lead to the requisite conditions through a combination of their high density and sequence thicknesses (Konhauser et al., 2002; Li et al., 2017; Robbins et al., 2019) (Figure S1 in Supporting Information S1). The BIF deposition peaked during 2.75–2.40 Ga and was distributed globally on the Neoarchean continental margins (Bekker et al., 2010; Konhauser et al., 2017), but their potential as the driving force of subduction initiation has not been evaluated.

BIFs are Precambrian marine deposits composed of alternating iron-oxide and chert bands (Klein, 2005). It is widely believed that the oxidation of Fe(II) in the highly anoxic Archean oceans is dominated by anoxygenic photoferrotrophy, although oxygenic photosynthesis may also contribute (Konhauser et al., 2017; Thompson et al., 2019). With the nutrient input from the proto-continent (Hao et al., 2020), photoferrotrophs thrived in the photic zone on the proto-continental margins, which have the highest contemporary primary productivity (Kappler et al., 2005; Konhauser et al., 2002; Thompson et al., 2019; Wollast, 2002). By harnessing the sunlight energy, the photoferrotrophic bacteria enzymatically oxidized Fe(II) to ferrihydrite (~$Fe(OH)_3$) and fixed CO_2 into biomass (Thompson et al., 2019) (Figure 1). Upon diagenetic solidification, ferrihydrite dehydrated and transformed to either hematite or magnetite in BIFs, with different mineralization pathways and condensed states (Li et al., 2017; Sun et al., 2015). Moreover, the iron oxides in Archean BIFs are mainly magnetite, and the hematite content has gradually exceeded the magnetite content since the Proterozoic (James, 1992; Li et al., 2017). The hematite in BIFs was directly dehydrated from its ferrihydrite precursor, maintaining an ultrafine crystal size (3–5 nm) and a high specific surface area (~200 m^2/g) so that it remained fluffy, similar to its oxyhydroxide precursor when settled on the seafloor (Sun et al., 2015). On the other hand, the active submarine volcanism and the released hydrothermal fluids in the Neoarchean promoted the formation of magnetite. These high Fe(II)-containing hydrothermal fluids would react with ferrihydrite on the seafloor to rapidly produce magnetite (Halevy et al., 2017; Li et al., 2017) (Figure 1). In contrast, magnetite nanoparticles make dense aggregation by magnetic interactions (Rebodos & Vikesland, 2010) (Figure S2 in Supporting Information S1). The magnetite would accumulate with silica to form thick BIFs on proto-continental margins. Also, these dense BIFs typically have a density 20%–40% higher than the lithosphere due to their high iron content (Konhauser et al., 2002; Thompson et al., 2019). Through their negative buoyancy, such BIF-hosted continental margins eventually develop into deep sedimentary basins (Figure 1), such as the Hamersley Basin in Western Australia (Trendall, 1983).

In addition to their dense state and high density, another important observation is the peak deposition of BIFs (2.75–2.40 Ga) (Bekker et al., 2010; Klein, 2005; Konhauser et al., 2002). Many large BIF-hosted basins (also called Superior-type BIFs) developed in this period have been identified (Bekker et al., 2010). They are found to be deposited in near-shore shelf environments and localized on continental margin basins (Konhauser et al., 2017; Trendall, 1983), which implies a widespread distribution of BIFs on global continental margins. Moreover, the depositional scales of BIFs were large and several giant BIFs in this period (2.75–2.40 Ga) were reported, such as the Hamersley Basin in Western Australia and the Transvaal Supergroup in South Africa. These two BIFs alone cover an area of over 10^5 km^2 and their thickness can reach kilometers (Robbins et al., 2019; Trendall, 1983).

During the peak deposition of BIFs, a depositional rate of ~1 km/Myr has been suggested by geochronological studies (Konhauser et al., 2002). This is equivalent to an iron depositional rate of ~45 mol $\cdot$ m^{-2} $\cdot$ yr^{-1} for the iron-rich BIFs with Fe wt% = 54.6% and $\rho = 4600$ kg/m^3 (Konhauser et al., 2002), which is close to the estimation given by recent laboratory experiments (Kappler et al., 2005; Thompson et al., 2019). Assuming all the Fe(III) in BIFs is the oxidation product of photoferrotrophy and using the estimated iron-oxidation rate of the photoferrotrophic bacteria ($1 - 3 \times 10^{-11}$ mol $\cdot$ cell^{-1} $\cdot$ yr^{-1}) (Konhauser et al., 2002; Maisch et al., 2019), a cell density of $3 - 9 \times 10^4$ cells/cm^3 over a 50-m-deep photic zone is adequate to sustain the above-mentioned BIF depositional rates. Such a cell density should be feasible since modern observations find that the bacterial population in the photic zone is typically on the order of 10^6 cells/cm^3 (Konhauser et al., 2002).

The high depositional rate (~1 km/Myr) implies that thick magnetite-rich BIFs would accumulate along continental margins within a few million years. The loading from these heavy sediments could be large enough to induce the rupture and subduction of the lithosphere along proto-continental margins. Based on these observations, we propose that the peak deposition of the heavy magnetite-rich BIFs in 2.75–2.40 Ga might have initiated the earliest subduction, thus indicating the origin of plate tectonics.

2. Geodynamic Models

We formulated 2-D thermomechanical models with viscoelastoplastic rock rheology to test the hypothesis that BIF deposition initiated subduction in the Neoarchean. Our reference model (Figure 2) consists of a 100-km-thick proto-continental plate (left side, 1,100 km wide) and a 100-km-thick oceanic plate (right side, 2,100 km wide). Presumably, crustal thickness variations before plate tectonics would have been gradual as they would have partially relaxed over millions of years. We assumed that before plate tectonics that there were regions of proto-continent composed of crust like tonalite–trondhjemite–granodiorite rocks with a density of ~2,900 kg/m^3 (Merriman et al., 2013). Consequently, a transition (from x = 1,000 km to x = 1,100 km) between the proto-continent and the oceanic domain is set (Figure 2a). The crustal thickness of the proto-continent and the oceanic plate is 30 and 15 km, respectively. A 40-km-thick "sticky air" layer above the lithosphere approximates the free surface (Crameri et al., 2012). The initial temperature field of the proto-continental and oceanic lithosphere is linearly distributed between 0°C and 1,550°C, while the sublithospheric temperature is homogeneous (1,550°C) and 200°C higher than the modern value (Rey et al., 2014) (Figure 2a). The width of the BIF-depositional area d_0 beneath the proto-continental margin is nominally set to 250 km (i.e., from x = 1,100 km to x = 1,350 km in Figure 2a), which is comparable to the basin width on modern mature passive margins (Cloetingh et al., 1982). BIF material is deposited on proto-continental margins at specified depositional rates (Figure 2). In this study, we assume that the photic zone on the Neoarchean continental margins dominated contemporary primary productivity, consistent with modern observations (Wollast, 2002). In the model, photoferrotrophic bacteria need to take up nutrients transported off the proto-continental margin (Hao et al., 2020) and produce BIF sediments. Their accumulation causes the localization of the modeled BIFs at the proto-continental margin. We established a 1-D ocean-mixing model (see Supporting Information S1) to determine the spatial distribution of the depositional rate $v_d(x)$ (Figure 2g). With a specific deposition rate $v_d(x)$ over a time Δt, BIF sediment of thickness, $h(x)$, is placed on top of the solid surface replacing the sticky air material:

$$h(x) = v_d(x)\Delta t \tag{1}$$

where Δt is the time interval to deposit BIFs. With a non-uniform depositional rate, a horizontally averaged value v_{ave} is used when comparing models. The yield stress of the marine sediments is believed to be low and we use the value determined from previous studies (Davis & von Huene, 1987) in the model (Table S1 in Supporting Information S1). Other details about the model can be found in Supporting Information S1.

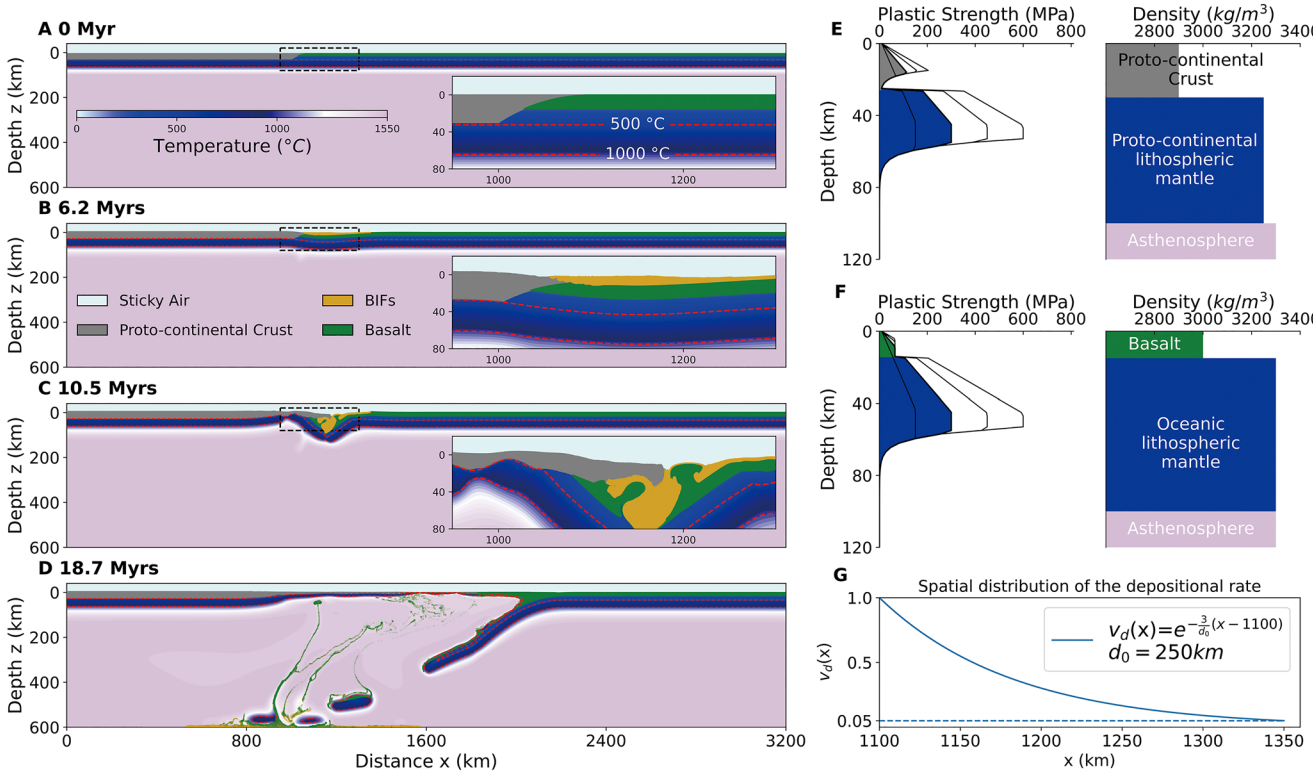

Figure 2. Computation of the subduction initiation process triggered by magnetite-rich BIFs. (a) The initial settings of the reference model. (b–d) The evolution snapshots in 6.2, 10.5, and 18.7 Myrs with isotherms shown with red dashed lines. The enlarged views of the depositional area (dashed box) in (a–c) are shown in the inset figures on the right. The crustal particles are superimposed on the original temperature field to distinguish the proto-continent (gray) from the ocean (green). BIF sediments are denoted in yellow. (e, f) Plastic-strength and density settings of the proto-continental plate (e) and the oceanic plate (f) in the reference model. The density of BIFs in the reference model is set to 4,600 kg/m^3. (g) The spatial distribution of the normalized depositional rate.

3. Results

3.1. Results of the Reference Model Case

For the reference model (Figure 2 and Figure S3 in Supporting Information S1), enough BIF sediments accumulate within ~9 Myrs to rupture the lithosphere when the peak BIF depositional rate is maintained at 1 km/Myr. Initially, the sedimentary loading is limited to moderate plate deflections (Figure 2b). However, as the sediments are weak, they flow horizontally, increasing the downward deflection of the lithosphere, which in turn leads to more localization of the high-density BIFs. The thickness of the sediments rapidly evolves away from the profile imposed by the ocean-mixing model (Figure 2g) to one with a more Gaussian shape (Figure 2b) and eventually one which is even more localized (Figure 2c). As the thickness of BIF sediments increases, the load eventually exceeds the yield strength of the lithosphere and the margin collapses (Figure 2c). After several million years, a retreating subduction slab starts at the position of plate rupture (Figure 2d). In the computations, when the lithosphere breaks and sinks into the mantle, BIF deposition shuts down and the horizontal-average BIF thickness at this time is recorded as the critical thickness (see Supporting Information S1 for details), which represents the minimum BIF thickness required to break the lithosphere.

3.2. Required BIF Thickness for Subduction Initiation With Different Mechanical Parameters

Compared with the reference model (Figure 2), thicker BIF sediment is required to induce subduction when either the yield stress or the thickness of lithosphere is increased (Figures 3a and 3b). When the maximum yield stress of the lithosphere increases from 150 to 600 MPa, the critical thickness of the BIF to rupture a 100-km-thick lithosphere varies from ~5 to ~12 km (Figure 3a). When the yield stress of the lithosphere is 300 MPa as recently estimated (Rey et al., 2014) and the lithospheric thickness increases from 75 to 125 km, the critical thickness changes from ~5 to ~11 km (Figure 3b). The thickness of the proto-continental crust can significantly influence

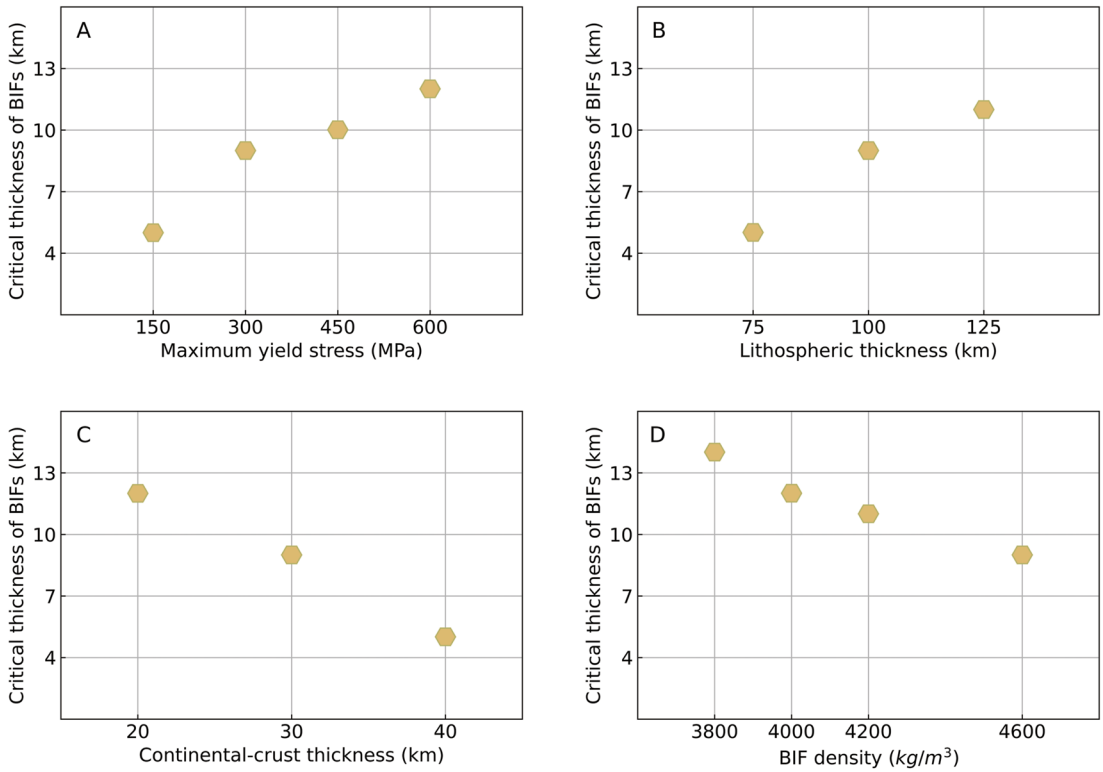

Figure 3. Critical thickness of BIFs required for subduction initiation with different mechanical and sediment parameters: (a) Yield stress of the lithosphere. (b) Lithospheric thickness. (c) Thickness of proto-continental crust. (d) Aggregate BIF density.

the buoyancy and strength of the lithosphere, but its value before plate tectonics is poorly constrained. We change the thickness from 20 to 40 km and the corresponding critical thickness of BIFs varies from ∼12 to ∼5 km (Figure 3c). Different densities of BIF from 4,600 kg/m^3 (iron-rich BIF, Fe wt% ≈ 55%) to 3,800 kg/m^3 (Fe wt% ≈ 35%) are tested, and the related critical thickness varies from ∼9 to ∼14 km (Figure 3d).

On modern passive margins, the thickness of the low-density silicate sediments can reach 15–20 km (Figure S4a in Supporting Information S1). However, with the deposition of BIFs, such a thickness is sufficient to induce subduction. In fact, the negative buoyancy of BIFs would drive it to subside continuously and deepen the basin (Trendall, 1983), so the upper bound of sedimentary thickness should be higher. Based on the computations and observed characteristics of BIFs in the Neoarchean (including its high density and depositional rate), magnetite-rich BIFs can trigger subduction over only several million years (∼10 Myrs).

3.3. Sensitivity Test for Other Parameters

The outcomes may also be affected by the degree to which deposition is localized, the sharpness of the ocean-continent transition, the sediment strength, and the time interval of deposition. When we change d_0 (depositional scale) from 150 to 300 km, the average depositional rate v_{ave} from 0.2 to 2 km/Myr, the width of the transitional area between proto-continent and ocean from 0 to 100 km, the friction coefficient of BIF from 0.0 to 0.1, and the time interval to deposit BIFs from 0.2 to 1 Myr, computations show that the critical thickness of BIFs is not substantially influenced (Figures S5a–S5e in Supporting Information S1).

4. Discussion

4.1. The Biological-Induced Origin of Plate Tectonics

The computations show that subduction initiation induced by magnetite-rich BIFs is physically plausible, and with a distinctive biomineralization genesis for BIFs implies a biologically induced origin of plate tectonics. As one of

the earliest energy metabolisms on Earth, the prosperity of photoferrotrophy presets the global tectonic environments. The photoferrotrophic bacteria used Fe(II) source in the anoxic seawater and efficiently metabolized it to acquire the necessary energy. Their thriving in the Neoarchean (Figure 4a) led to the massive deposition of ferrihydrite on the proto-continental margins. Meanwhile, vigorous submarine volcanism in the Neoarchean (Isley & Abbott, 1999) should have significantly increased the supply of hydrothermal Fe(II) to the photic zone, which has reacted with the ferrihydrite directly to make dense magnetite deposition on the seafloor at the proto-continental margins (Halevy et al., 2017; Li et al., 2017). The synchronous appearance of the anoxic oceanic environment (Kump & Barley, 2007), the high Fe(II)-oxidizing rate from thriving photoferrotrophs (Konhauser et al., 2002), and the abundant hydrothermal Fe(II) alternations in the Neoarchean (Isley & Abbott, 1999) satisfied the conditions to deposit massive magnetite-rich BIFs rapidly (Halevy et al., 2017; Li et al., 2017) (Figure 4b). We propose that these high-density sediments on the proto-continental margins broke the lithosphere, induced the earliest subduction, and initiated plate tectonics.

The BIFs that subducted presumably would have sunk into the deeper mantle; the transport of BIFs into the lower mantle has previously been suggested as a mechanism to form the ultralow-velocity zones (ULVZs) at the core-mantle boundary (Dobson & Brodholt, 2005). Interestingly, ULVZs are generally hundreds of kilometers wide, tens of kilometers high, and thought to be composed of high density, Fe-rich material (Bower et al., 2011), not unlike the BIF sedimentary packages required to trigger subduction initiation.

The distinctive biogeochemical formation of magnetite gradually shut down after the Neoarchean. The oxidation of the ocean since the early Paleoproterozoic (Figure 4c) has significantly depressed the dissolved Fe(II) in the seawater, reducing the contribution of photoferrotrophy to primary production and ferric oxide deposition (Li et al., 2017). After the Great Oxidation Event (GOE) (Figure 4c), the emerging oxygenic photosynthesis gradually surpassed the anaerobic photoferrotrophy (Figure 4a) so that the BIF deposition was significantly decreased (Bekker et al., 2010) (Figure 4b) and contained less magnetite (James, 1992; Li et al., 2017). On modern continental margins, the marine photic zone overlaps subduction zones, a similar scene we propose at the onset time of the global plate tectonics in the Neoarchean (Figure S4b in Supporting Information S1). Following the Neoarchean, the low-density silicate deposits replaced the heavy BIFs, and sediment-induced subduction initiation shut down by which time new subduction zones could continuously formed by mechanisms now seen in the plate tectonic system (Gurnis, 2023; Stern & Gerya, 2018).

4.2. The Onset Time of Plate Tectonics

Our model implies a timing for the start of global plate tectonics. Despite long-standing discussion on this timing (Cawood et al., 2018; Condie & Kröner, 2008; Korenaga, 2013) and possible tectonic styles (T. Gerya, 2019; Sobolev & Brown, 2019; Stern, 2020; Yao et al., 2021), most studies accept that the onset of modern-type plate tectonics is coeval with the onset of the earliest subduction (T. V. Gerya et al., 2015; Rey et al., 2014). Based on our model, the earliest subduction started on global continental margins and was triggered by the rapid BIF deposition during 2.75–2.40 Ga, which is well supported by many contemporary plate-tectonic indicators and geological events. During the transition from the Neoarchean to Paleoproterozoic, volcanism recorded by large igneous provinces (LIPs) gradually shifted from submarine to subaerial (Kump & Barley, 2007) (Figure 4d). Since submarine volcanism is more reductive than subaerial volcanism (Kump & Barley, 2007), the preponderance of submarine LIPs in the Archean is consistent with the anoxic environment at that time and the related submarine hydrothermal alteration could provide Fe(II) for the rapid mineralization of magnetite during peak BIF deposition (Li et al., 2017). Once plate tectonics began, the frequent subduction of the oceanic lithosphere would make submarine LIPs preferentially destroyed and short-lived (Kump & Barley, 2007). Therefore, the decrease of submarine-volcano proportion since the Neoarchean-Paleoproterozoic transition (Figure 4d) probably corresponds to the time when BIF first induced the subduction of the oceanic plates. The existence of subduction is supported by the first identification of the Archean paired metamorphic units which are spatially and temporally linked (2.54–2.50 Ga) in the granite-greenstone belt (Huang et al., 2020) (Figure 4e). With the establishment of subduction zones, large-scale horizontal plate movement would start and is consistent with recent paleomagnetic reconstructions suggesting such movements (>5,000 km) between cratonic blocks already existed by ca. 2.7–2.4 Ga (Cawood et al., 2018) (Figure 4e). The crustal-growth peaked in the Neoarchean (2.7–2.5 Ga) (Condie et al., 2009) (Figure 4e) also supports our scenario. Arc magmatism resulting from the earliest subduction would strongly promote the formation of continental crust and provides a reasonable interpretation for the

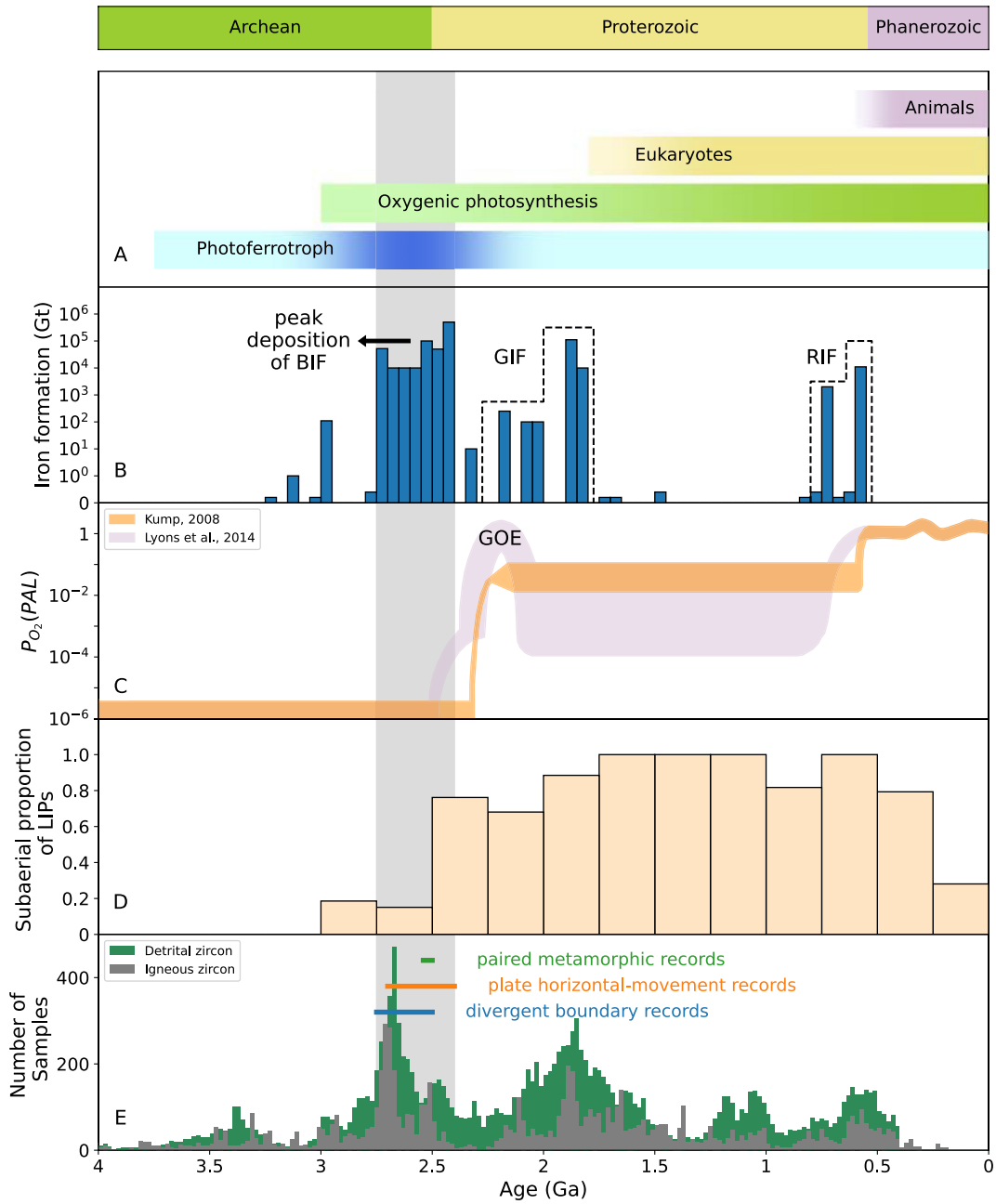

Figure 4. Important geological events during the Archean-Proterozoic transition period. (a) The evolutionary timeline of the biosphere (Knoll & Nowak, 2017). (b) Frequency histogram of the iron formation (IF) with 50-Myr-wide bars (Bekker et al., 2010). Most IFs before 2.4 Ga belong to BIF (Bekker et al., 2010). The sediments in 2.3–0.8 Ga and 0.8–0.56 Ga are dominated by the granular iron formation (GIF) and the Rapitan-type iron formation (RIF), respectively (Bekker et al., 2010). (c) Evolution models of atmospheric oxygen content suggested by Kump (2008) (purple) and Lyons et al. (2014) (orange). P_{O_2}: atmospheric partial pressure of oxygen relative to the present atmospheric level (PAL); GOE: Great Oxygenation Event. (d) Secular variation in proportion of subaerial LIPs (Kump & Barley, 2007). The total large igneous provinces (LIPs) are divided into two types, the subaerial LIPs and the submarine ones. (e) Distribution of the detrital and the igneous zircons reported by Condie et al. (2009) and other plate-tectonic indicators in the Neoarchean.

rapid crustal growth during this period (Condie et al., 2009), although some numerical studies suggest that subduction with hotter Archean mantle may be inefficient in producing continental crust (Perchuk et al., 2019).

Convergent boundaries such as subduction zones are not the only proxy of plate tectonics, as divergent boundary records such as mid-ocean ridges (MORs) are proxies as well. The appearance of the oldest divergent-boundary

records in the Neoarchean (Cawood et al., 2018; Condie & Kröner, 2008) (Figure 4e) supports the inferred start of plate tectonics. Such records can be traced back to 2.75–2.5 Ga in several Archean cratons (Cawood et al., 2018). The appearance of nascent MORs means that more Fe(II)-rich fluids would be available for magnetite mineralization. Because of the higher elevation of these oceanic ridges compared with oceanic basins, the released hydrothermal Fe(II) fluids would reach the upper ocean layer close to the BIF-deposition depth more easily (Li et al., 2017), facilitating the rapid and massive deposition of magnetite-rich BIFs.

5. Conclusions

In this model of plate tectonics initiation, we find the extraordinary role of photoferrotrophic bacteria on early Earth. They effectively oxidize the dissolved ferrous iron and aggregate the resulting ferric oxides onto proto-continental margins, which were turned to dense magnetite by further reaction of Fe(II) from the submarine hydrothermal fluids. These high-density banded iron sediments could break the proto-continental margins to start subduction and kick-started plate tectonics. Their peak deposition in 2.75–2.40 Ga constrains the time plate tectonics started. This unique biogeochemical cycle with the biomineralization of amorphous ferrihydrite and the magnetization by the addition of hydrothermal Fe(II) fluids could only happen on Earth and only once during this period. The model implies that prosperous photoferrotrophy in the Neoarchean is the reason why Earth is the only planet with plate tectonics. In this sense, life has played an even more important role in uniquely shifting the tectonic style of Earth to a plate tectonic system.

Data Availability Statement

The code Ellipsis is available at CIG (https://geodynamics.org/resources/ellipsis3d) or can be downloaded from Github (https://github.com/geodynamics/ellipsis3d/archive/refs/tags/v1.0.2.zip). The sedimentary thickness data is from NOAA (https://www.ngdc.noaa.gov/mgg/sedthick/data/version3/GlobSed.zip). The chlorophyll-a data is from NASA OceanColor (https://oceancolor.gsfc.nasa.gov/l3/) by clicking the button called "Extract or Download L3 Data." The data of subduction boundaries is from EarthByte (https://www.earthbyte.org/webdav/ftp/Data_Collections/Merdith_etal_2021_ESR/SM2-Merdith_et_al_1_Ga_reconstruction_v1.1.zip).

Acknowledgments
S.Z., Y.L., and W.L. acknowledge financial support from the Strategic Priority Research Program of Chinese Academy of Sciences (XDB41000000). S.Z. and W.L. are also partially supported by Natural Science Foundation of China (42241117 and 41820104004). M.G. was supported by NSF OCE–2049086.

References

Bekker, A., Slack, J. F., Planavsky, N., Krapez, B., Hofmann, A., Konhauser, K. O., & Rouxel, O. J. (2010). Iron formation: The sedimentary product of a complex interplay among mantle, tectonic, oceanic, and biospheric processes. *Economic Geology*, *105*(3), 467–508. https://doi.org/10.2113/gsecongeo.105.3.467

Bower, D. J., Wicks, J. K., Gurnis, M., & Jackson, J. M. (2011). A geodynamic and mineral physics model of a solid-state ultralow-velocity zone. *Earth and Planetary Science Letters*, *303*(3–4), 193–202. https://doi.org/10.1016/j.epsl.2010.12.035

Cawood, P. A., Hawkesworth, C. J., Pisarevsky, S. A., Dhuime, B., Capitanio, F. A., & Nebel, O. (2018). Geological archive of the onset of plate tectonics. *Philosophical Transactions of the Royal Society A: Mathematical, Physical & Engineering Sciences*, *376*(2132), 20170405. https://doi.org/10.1098/rsta.2017.0405

Cloetingh, S. A. P. L., Wortel, M. J. R., & Vlaar, N. J. (1982). Evolution of passive continental margins and initiation of subduction zones. *Nature*, *297*(5862), 139–142. https://doi.org/10.1038/297139a0

Condie, K. C., Belousova, E., Griffin, W. L., & Sircombe, K. N. (2009). Granitoid events in space and time: Constraints from igneous and detrital zircon age spectra. *Gondwana Research*, *15*(3–4), 228–242. https://doi.org/10.1016/j.gr.2008.06.001

Condie, K. C., & Kröner, A. (2008). When did plate tectonics begin? Evidence from the geologic record. In *Special paper 440: When did plate tectonics begin on planet Earth?* (Vol. 440, pp. 281–294). Geological Society of America. https://doi.org/10.1130/2008.2440(14)

Crameri, F., Schmeling, H., Golabek, G. J., Duretz, T., Orendt, R., Buiter, S. J. H., et al. (2012). A comparison of numerical surface topography calculations in geodynamic modelling: An evaluation of the 'sticky air' method. *Geophysical Journal International*, *189*(1), 38–54. https://doi.org/10.1111/j.1365-246X.2012.05388.x

Davis, D. M., & von Huene, R. (1987). Inferences on sediment strength and fault friction from structures at the Aleutian Trench. *Geology*, *15*(6), 517. https://doi.org/10.1130/0091-7613(1987)15<517:IOSSAF>2.0.CO;2

Dobson, D. P., & Brodholt, J. P. (2005). Subducted banded iron formations as a source of ultralow-velocity zones at the core–mantle boundary. *Nature*, *434*(7031), 371–374. https://doi.org/10.1038/nature03430

Erickson, S. G. (1993). Sedimentary loading, lithospheric flexure, and subduction initiation at passive margins. *Geology*, *21*(2), 125. https://doi.org/10.1130/0091-7613(1993)021<0125:SLLFAS>2.3.CO;2

Escartín, J., Hirth, G., & Evans, B. (2001). Strength of slightly serpentinized peridotites: Implications for the tectonics of oceanic lithosphere. *Geology*, *29*(11), 1023. https://doi.org/10.1130/0091-7613(2001)029<1023:SOSSPI>2.0.CO;2

Gerya, T. (2019). Geodynamics of the early Earth: Quest for the missing paradigm. *Geology*, *47*(10), 1006–1007. https://doi.org/10.1130/focus102019.1

Gerya, T. V., Stern, R. J., Baes, M., Sobolev, S. V., & Whattam, S. A. (2015). Plate tectonics on the Earth triggered by plume-induced subduction initiation. *Nature*, *527*(7577), 221–225. https://doi.org/10.1038/nature15752

Gurnis, M. (2023). An evolutionary perspective on subduction initiation. In J. C. Duarte (Ed.), *Dynamics of plate tectonics and mantle convection* (pp. 357–383). Elsevier. https://doi.org/10.1016/B978-0-323-85733-8.00003-2

Halevy, I., Alesker, M., Schuster, E. M., Popovitz-Biro, R., & Feldman, Y. (2017). A key role for green rust in the Precambrian oceans and the genesis of iron formations. *Nature Geoscience*, *10*(2), 135–139. https://doi.org/10.1038/ngeo2878

Hansen, V. L. (2007). Subduction origin on early Earth. *Hypothesis: Geology*, *35*(12), 1059. https://doi.org/10.1130/G24202A.1

Hao, J., Knoll, A. H., Huang, F., Hazen, R. M., & Daniel, I. (2020). Cycling phosphorus on the Archean Earth: Part I. Continental weathering and riverine transport of phosphorus. *Geochimica et Cosmochimica Acta*, *273*, 70–84. https://doi.org/10.1016/j.gca.2020.01.027

Huang, B., Kusky, T. M., Johnson, T. E., Wilde, S. A., Wang, L., Polat, A., & Fu, D. (2020). Paired metamorphism in the Neoarchean: A record of accretionary-to-collisional orogenesis in the North China Craton. *Earth and Planetary Science Letters*, *543*, 116355. https://doi.org/10.1016/j.epsl.2020.116355

Isley, A. E., & Abbott, D. H. (1999). Plume-related mafic volcanism and the deposition of banded iron formation. *Journal of Geophysical Research*, *104*(B7), 15461–15477. https://doi.org/10.1029/1999JB900066

James, H. L. (1992). Chapter 11 Precambrian iron-formations: Nature, origin, and mineralogic evolution from sedimentation to metamorphism. In *Orthodontic treatment of class III malocclusion* (Vol. 1990, pp. 543–589). https://doi.org/10.1016/S0070-4571(08)70573-9

Kappler, A., Pasquero, C., Konhauser, K. O., & Newman, D. K. (2005). Deposition of banded iron formations by anoxygenic phototrophic Fe(II)-oxidizing bacteria. *Geology*, *33*(11), 865. https://doi.org/10.1130/G21658.1

Klein, C. (2005). Some Precambrian banded iron-formations (BIFs) from around the world: Their age, geologic setting, mineralogy, metamorphism, geochemistry, and origins. *American Mineralogist*, *90*(10), 1473–1499. https://doi.org/10.2138/am.2005.1871

Knoll, A. H., & Nowak, M. A. (2017). The timetable of evolution. *Science Advances*, *3*(5), 1–14. https://doi.org/10.1126/sciadv.1603076

Konhauser, K. O., Hamade, T., Raiswell, R., Morris, R. C., Grant Ferris, F., Southam, G., & Canfield, D. E. (2002). Could bacteria have formed the Precambrian banded iron formations? *Geology*, *30*(12), 1079. https://doi.org/10.1130/0091-7613(2002)030<1079:CBHFTP>2.0.CO;2

Konhauser, K. O., Planavsky, N., Hardisty, D., Robbins, L., Warchola, T., Haugaard, R., et al. (2017). Iron formations: A global record of Neoarchaean to Palaeoproterozoic environmental history. *Earth-Science Reviews*, *172*, 140–177. https://doi.org/10.1016/j.earscirev.2017.06.012

Korenaga, J. (2013). Initiation and evolution of plate tectonics on Earth: Theories and observations. *Annual Review of Earth and Planetary Sciences*, *41*(1), 117–151. https://doi.org/10.1146/annurev-earth-050212-124208

Kump, L. R. (2008). The rise of atmospheric oxygen. *Nature*, *451*(7176), 277–278. https://doi.org/10.1038/nature06587

Kump, L. R., & Barley, M. E. (2007). Increased subaerial volcanism and the rise of atmospheric oxygen 2.5 billion years ago. *Nature*, *448*(7157), 1033–1036. https://doi.org/10.1038/nature06058

Li, Y.-L., Konhauser, K. O., & Zhai, M. (2017). The formation of magnetite in the early Archean oceans. *Earth and Planetary Science Letters*, *466*, 103–114. https://doi.org/10.1016/j.epsl.2017.03.013

Lyons, T. W., Reinhard, C. T., & Planavsky, N. J. (2014). The rise of oxygen in Earth's early ocean and atmosphere. *Nature*, *506*(7488), 307–315. https://doi.org/10.1038/nature13068

Maisch, M., Lueder, U., Laufer, K., Scholze, C., Kappler, A., & Schmidt, C. (2019). Contribution of microaerophilic iron(II)-oxidizers to iron(III) mineral formation. *Environmental Science & Technology*, *53*(14), 8197–8204. https://doi.org/10.1021/acs.est.9b01531

Merriman, J. D., Whittington, A. G., Hofmeister, A. M., Nabelek, P. I., & Benn, K. (2013). Thermal transport properties of major Archean rock types to high temperature and implications for cratonic geotherms. *Precambrian Research*, *233*, 358–372. https://doi.org/10.1016/j.precamres.2013.05.009

Mulyukova, E., & Bercovici, D. (2017). Formation of lithospheric shear zones: Effect of temperature on two-phase grain damage. *Physics of the Earth and Planetary Interiors*, *270*, 195–212. https://doi.org/10.1016/j.pepi.2017.07.011

Perchuk, A. L., Zakharov, V. S., Gerya, T. V., & Brown, M. (2019). Hotter mantle but colder subduction in the Precambrian: What are the implications? *Precambrian Research*, *330*, 20–34. https://doi.org/10.1016/j.precamres.2019.04.023

Poirier, J. P. (1980). Shear localization and shear instability in materials in the ductile field. *Journal of Structural Geology*, *2*(1–2), 135–142. https://doi.org/10.1016/0191-8141(80)90043-7

Rebodos, R. L., & Vikesland, P. J. (2010). Effects of oxidation on the magnetization of nanoparticulate magnetite. *Langmuir*, *26*(22), 16745–16753. https://doi.org/10.1021/la102461z

Rey, P. F., Coltice, N., & Flament, N. (2014). Spreading continents kick-started plate tectonics. *Nature*, *513*(7518), 405–408. https://doi.org/10.1038/nature13728

Robbins, L. J., Funk, S. P., Flynn, S. L., Warchola, T. J., Li, Z., Lalonde, S. V., et al. (2019). Hydrogeological constraints on the formation of Palaeoproterozoic banded iron formations. *Nature Geoscience*, *12*(7), 558–563. https://doi.org/10.1038/s41561-019-0372-0

Sobolev, S. V., & Brown, M. (2019). Surface erosion events controlled the evolution of plate tectonics on Earth. *Nature*, *570*(7759), 52–57. https://doi.org/10.1038/s41586-019-1258-4

Stern, R. (2020). The Mesoproterozoic single-lid tectonic episode: Prelude to modern plate tectonics. *Geological Society of America Today*, *30*(12), 4–10. https://doi.org/10.1130/GSATG480A.1

Stern, R. J., & Gerya, T. (2018). Subduction initiation in nature and models. *A Review: Tectonophysics*, *746*, 173–198. https://doi.org/10.1016/j.tecto.2017.10.014

Sun, S., Konhauser, K. O., Kappler, A., & Li, Y.-L. (2015). Primary hematite in Neoarchean to Paleoproterozoic oceans. *Geological Society of America Bulletin*, *127*(5–6), 850–861. https://doi.org/10.1130/B31122.1

Thielmann, M., & Kaus, B. J. P. (2012). Shear heating induced lithospheric-scale localization: Does it result in subduction? *Earth and Planetary Science Letters*, *359–360*, 1–13. https://doi.org/10.1016/j.epsl.2012.10.002

Thompson, K. J., Kenward, P. A., Bauer, K. W., Warchola, T., Gauger, T., Martinez, R., et al. (2019). Photoferrotrophy, deposition of banded iron formations, and methane production in Archean oceans. *Science Advances*, *5*(11), eaav2869. https://doi.org/10.1126/sciadv.aav2869

Trendall, A. F. (1983). The Hamersley basin: Developments in Precambrian geology. *Iron-Formation Facts and Problems*, *6*, 69–129. https://doi.org/10.1016/S0166-2635(08)70042-2

Wollast, R. (2002). Continental margins—Review of geochemical settings. In *Ocean margin systems* (pp. 15–31). Springer Berlin Heidelberg. https://doi.org/10.1007/978-3-662-05127-6_2

Yao, J., Cawood, P. A., Zhao, G., Han, Y., Xia, X., Liu, Q., & Wang, P. (2021). Mariana-type ophiolites constrain the establishment of modern plate tectonic regime during Gondwana assembly. *Nature Communications*, *12*(1), 4189. https://doi.org/10.1038/s41467-021-24422-z

References From the Supporting Information

Karato, S.-I., & Wu, P. (1993). Rheology of the upper mantle: A synthesis. *Science*, *260*(5109), 771–778. https://doi.org/10.1126/science.260.5109.771

Li, Y.-L. (2014). Micro- and nanobands in late Archean and Palaeoproterozoic banded-iron formations as possible mineral records of annual and diurnal depositions. *Earth and Planetary Science Letters*, *391*, 160–170. https://doi.org/10.1016/j.epsl.2014.01.044

McCall, K. K., & Martin, C. E. (1991). Chlorophyll concentrations and photosynthesis in three forest understory mosses in northeastern Kansas. *The Bryologist*, *94*(1), 25. https://doi.org/10.2307/3243713

Moresi, L., Dufour, F., & Mühlhaus, H.-B. (2003). A Lagrangian integration point finite element method for large deformation modeling of viscoelastic geomaterials. *Journal of Computational Physics*, *184*(2), 476–497. https://doi.org/10.1016/S0021-9991(02)00031-1

O'Neill, C., Moresi, L., Müller, D., Albert, R., & Dufour, F. (2006). Ellipsis 3D: A particle-in-cell finite-element hybrid code for modelling mantle convection and lithospheric deformation. *Computers & Geosciences*, *32*(10), 1769–1779. https://doi.org/10.1016/j.cageo.2006.04.006

Ranalli, G. (1995). *Rheology of the Earth* (2nd ed.). Springer Science & Business Media.